Defence Science Journal, Vol. 75, No. 5, September 2025, pp. 570-580, DOI : 10.14429/dsj.20580

Low Cross Polarized and Matching Improved Ground Extended Defected Structure Wearable Antenna for Tactical Battlefield Communications

S. Anand[$,*], Sivasankar Ganesan[#], D. Sujitha[$] and S. Vigneshwari[$]

[$]*Mepco Schlenk Engineering College, Sivakasi - 626 005, India*
[#]*Amrita School of Engineering, Coimbatore - 641 112, India*
[*]*E-mail: sanand@mepcoeng.ac.in*

ABSTRACT

In this paper, a flexible slot antenna of size 36 mm × 40 mm × 3 mm with high gain and low Specific Absorption Rate (SAR) is proposed. Wearable Antenna (WA) must achieve low cross-polarization, efficient impedance matching, high radiation gain, reduced SAR, and minimal return loss to ensure user safety and reliable performance in tactical communication environments. The proposed flexible antenna features a radiating patch with a combination of square and circular slots, fed by a Microstrip Patch (MSPA). Additionally, the extended ground plane incorporates a circular slot as part of a Defective Ground Structure (DGS). The circular slot is strategically positioned for optimal impedance matching and analysed. Textile felt is employed as the substrate, resulting in a return loss of less than -40 dB at 5.8 GHz. It is designed for tactical battlefield communications within the 5.725-5.875 GHz range, offering a bandwidth greater than 150 MHz and exhibiting a low cross-polarization radiation pattern. Simulated and measured *S*11 results demonstrate good impedance matching, supported by consistent gain variation across different theta angles. The far-field gain pattern comparison, with and without the circular slot DGS, along with SAR measurements at various distances, validates the antenna's performance and safety for practical use. The proposed antenna exhibits a gain of 8 dBi and maintains a SAR value below the IEEE standard, while achieving desirable antenna parameters.

Keywords: Circular slot; Extended DGS; low SAR; Wearable antennas; Tactical battlefield communications

NOMENCLATURE

BAN	: Body area network
BW	: Bandwidth
DGS	: Defective ground structure
dB	: Decibels
dBi	: Decibels relative to isotropic radiator
E	: Electric field
ε_r	: Relative Permittivity
Γ	: Reflection Coefficient
GHz	: Giga hertz
IEEE	: Institute of Electrical and Electronics Engineers
ISM	: Industrial, scientific and medical band
ITU	: International telecommunication union
$\mathcal{LC}$	: Inductance and capacitance
MHz	: Mega hertz
MIMO	: Multi input multi output
MSPA	: Microstrip patch antenna
RFID	: Radio frequency
*S*11	: Reflection coefficient
SAR	: Specific absorption rate
σ	: Conductivity
TM	: Transverse Magnetic Mode
UHF	: Ultra high frequency
VSWR	: Voltage standing wave ratio
WA	: Wearable antennas
WAN	: Wide area network
WiFi	: Wireless fidelity
WiMAX	: Worldwide Interoperability for Microwave Access

Received : 12 September 2024, Revised : 05 January 2025
Accepted : 15 March 2025, Online published : 01 September 2025

1. INTRODUCTION

The design of WAs ensures their functionality when worn on the human body. They are essential for various uses, including tactical warfare communications. These antennas must be lightweight, flexible, and able to conform to the contours of the body while maintaining the highest possible levels of signal transmission and reception efficiency. In tactical battlefield communications, WAs are used to make sure that military personnel can reliably and consistently talk to each other. Figure 1 illustrates the schematic of a WA for tactical battlefield communications.

This makes it possible for instant data exchange, voice contact, and integration with command centers. Moreover, a WA must achieve low cross-polarization, efficient impedance matching, high radiation gain, reduced SAR, and minimal return loss to ensure user safety and reliable performance in tactical communication environments. Often, manufacturers integrate these devices into clothes, caps, and other technical gear to minimize their restriction on the wearer's movement and comfort. These devices are constructed using flexible materials to facilitate their incorporation into clothing when

positioned on different body areas, such as the chest, wrist, head, etc., thereby requiring flexible materials in a low-profile design. WA has garnered significant interest recently due to its desirable characteristics, including affordability, light weight, and adaptability. WA's design is always difficult because of its small size requirements, structural deformation and coupling to the body, fabrication's complexity, and demand of accuracy. These antennas thus have to operate with low SAR in close proximity to the human body, spanning a range of areas. The integration of wireless units and WA has associated challenges, i.e., flexibility, robustness, and cost-effectiveness, while still exhibiting RF performance similar to that of their rigid counterparts. Microstrip Patch Antennas (MSPAs) are suitable for microwave frequencies where conventional bulky antennas are impractical, offering advantages such as lightweight, compactness, flexibility, and mechanical resilience making them ideal for modern flexible wearable antennas.

Flexible WA is broadly categorized based on frequency of applications (ISM, WAN, BAN, WiFi, WiMAX, etc.). Also, they may be classified into antenna design, i.e., microstrip, dipole, loop, etc., and substrate used i.e., textile, felt, jeans, etc. DGS refers to slots or defects incorporated into an antenna's ground plane that are used to improve various antenna properties such as narrow bandwidth, lower cross polarization, lower gain, and so on. Based on the location of DGS, the antenna ground plane can be divided into two parts (i) ground underneath the patch (i.e., ground directly under the patch) and (ii) extended ground (i.e., ground not directly under the patch). The majority of DGS structures are found beneath patches, and some research claims that DGS structures can be found in both portions. There were no DGS slots in the extended ground area, to the author's knowledge.

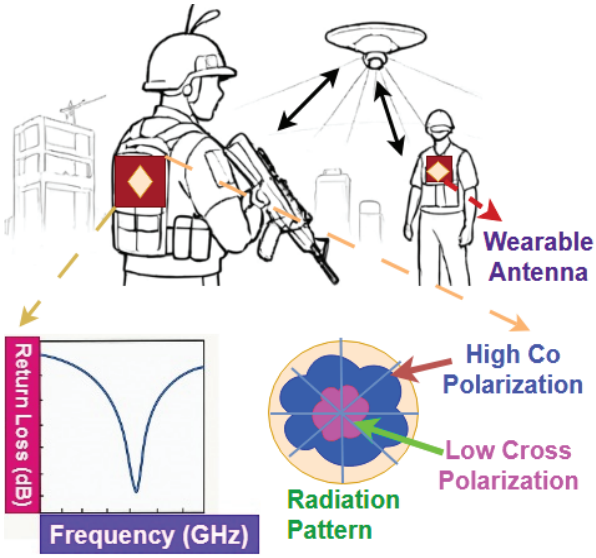

Figure 1. Schematic illustration of the proposed wearable antenna designed for tactical battlefield communications.

The demand for WA in various applications has expanded dramatically in recent years. Various approaches and constructions have been proposed to address antenna problems near the human body[1]. A three-dimensional, corrugated earth structure is described as miniaturization technology for microstrip antennas is used to WA. A corrugated ground structure in a textile embodiment is achieved by folding the entire ground plane locally. Raise it beneath each of the two radiating edges of the microstrip antenna[2]. A Ku, K, and Ka-band metamaterial absorber made entirely of textiles is described[3]. In this, square-shaped split ring resonators serve as the foundation for the metamaterial absorber. The selection of design parameters is predicated on felt dielectric substances and widely utilized electronic textiles operating at 13.1 and 31.13 GHz. For use in military applications, a wearable conformal antenna[4] that is small, low-profile, and circularly polarized is constructed using a metasurface that operates in the X-band.

This work focuses on the additional resonances that arise from surface wave propagation on a modified metasurface, which provides a wide axial ratio bandwidth and high gain wide impedance bandwidth. This antenna is flexible and precisely fits the human structure. The study[5] reported the use of a flexible and small wearable pear-shaped super high-frequency antenna with defensive beacon technology for precise location detection and tracking. The SAR simulation is achieved by wearing this antenna on a soldier's uniform. A prototype is built and validated through experimentation. The antenna's overall shape is harmonious, demonstrating the vital situational awareness and data-sharing capabilities needed for defense beacon technology. The paper[6] describes the design and development of a small, geometrically simple, wideband, high-gain antenna for V-band communication systems.

The antenna is created using a standard circular patch, which is then altered using a second circular patch that uses fractals. The antenna's bandwidth is also greatly increased with the inclusion of three elliptical-shaped patches. They etch a circular slot in the radiator to improve the antenna's emission pattern. The study[7] employs a thin layer of graphene to cover a flame retardant-4 (FR-4) glass epoxy substrate and operates at 2.45 GHz. It focuses on constructing rectangular patch antennas with various ground plane widths, including short edge, double ground, and triple ground. With finite ground planes, diffraction of radiation from the ground plane's edges occurs, causing variations in the radiation pattern, radiation conductance, and resonant frequency. Two patterns of pattern-reconfigurable WA for body-centric wireless communications are discussed[8]. In[9], the authors demonstrated a planar, small, dual-band antenna for 2.45-5.85 GHz wireless body-area network applications using a semi-flexible substrate. Based on graphene, a low-profile circularly polarized WA with flexible performance and low SAR is reported[10].

A wearable dual-band belt antenna is designed to provide steady performance in both on-and off-body settings[11]. Researchers utilize a wearable all-textile MSPA for body-centric communications in the dual bands of the medical body area network (2.36–2.40 GHz) and WiMAX (3.4–3.6 GHz)[12]. A study has been conducted on the development of antennas for wearable applications. The researchers have successfully created new antennas on fabric substrates that can be used to communicate with both in-body and outside-the-body sensors[13]. The antenna's integrated high-impedance surface is designed to work at 2.45 GHz for wearable applications and is compact and sturdy. They are made of a fabric that is extremely flexible[14]. Researchers are currently studying a new combination of loop

and dipole antennas in a Yagi-like structure to implement a WA[15]. This textile antenna has been seamlessly incorporated into a smart glove, along with a compact UHF-RFID reader. A method described in[16] utilizes characteristic mode analysis to estimate the forward directivity by subtracting the active mode based on the difference in modal significance curves. This enhanced the efficiency of the antenna gain optimization during the design process. The study[17] introduces a WA that leverages fractal geometry and electromagnetic band gap structures to improve the performance of WLAN applications and minimize interference. The antenna is made to be strong, effective, and hidden. At a frequency of 2.45 GHz and in an open space, the antenna has a front-to-back ratio of 13 dB, a gain of 7.86 dBi compared to an isotropic radiator, and a radiation efficiency of 90.35 %. Its bandwidth is 32 MHz when the resistance is matched. It also has a SAR of 0.302 W/kg for 1 g of tissue and 0.1423 W/kg for 10 g of tissue.

The main goal of the study[18] is to make a low-profile Archimedean spiral antenna. The goal of this antenna is to make it work better and more efficiently by using a small DGS as a reflector. This design works in the frequency range of 1.6 GHz to 6 GHz and is 60 % shorter than standard cavity-backed spiral antennas. Additionally, the study[19] talks about the creation of a wideband fabric antenna made for ultra-wideband uses, mainly medical ones. This antenna sends out waves in a broadside pattern and has a frequency range of 2.3 to 8 GHz. Some recent works have explored innovative antenna solutions for advanced wireless applications. In[20], a circularly polarized MIMO antenna system was developed using characteristic mode theory to support millimeter-wave 5G communications. In[21], an ultra-miniaturized UWB WA was proposed for e-health monitoring. This design ensures reliable on-body performance, even under bending and body proximity conditions, making it suitable for continuous health data acquisition.

However, from the previous works, it is learned that the simultaneous achievement of high gain, low SAR, and very low return loss in the design of WA along with other required antenna parameters is crucial to achieve. Specifically, these requirements are essential in tactical battlefield communications operating 5.725-5.875 GHz range in the C-band. This paper contributes a wearable, flexible, slot, DGS MSPA of size 36 mm × 40 mm × 3 mm with high gain, low SAR, and very low return loss (best matching). The proposed antenna operates in the C band from 5.725 GHz to 5.875 GHz with a center frequency of 5.8 GHz and a 150 MHz BW. From the overview of the frequencies within the ISM band and highlights key radio frequency allocations as outlined in Article 5 of the ITU Radio Regulations (edition 2012), the 5.8 GHz band is highly valuable for tactical battlefield communications due to its combination of high data rates, resilience to interference, flexibility for mobile and satellite use, and compatibility with compact and portable devices, all of which are essential for modern military operations. Following are the contributions and highlights of this research paper.

- Optimally located circular slot DGS in the extended ground
- Structuring both circular and rectangular slots in the center of the radiating patch
- Reducing the cross-polarization and simultaneous achievement of high gain along with reduced mismatching
- Antenna development according to ITU-R, flexible WA runs over a frequency range of 5.725 to 5.875 GHz, with a center frequency of 5.8 GHz and a BW of 150 MHz in C band and fulfilled low SAR specified by IEEE.

2. MODELLING OF DGS IN EXTENDED GROUND

2.1 DGS in Extended Ground

Traditional MSPA offers numerous benefits, but it also has several drawbacks, such as a single working frequency, narrow impedance BW, low gain, greater size, and polarization issues. A variety of approaches for improving MSPA parameters have been described, including stacking, various feeding techniques, frequency-selective surfaces, photonic band gaps, metamaterials, and so on. DGS has gained popularity among all the strategies mentioned for boosting the parameters due to its easy structural design. DGS refers to etched slots or faults on the ground plane of MSPA. DGS can refer to a single or several defects on the ground plane. The majority of the DGS is said to be completely or partially below the MSPA.

DGS has been employed in the field of MSPA to improve the radiation properties by suppressing higher mode harmonics, mutual coupling between neighboring elements, and cross-polarization. The DGS has been integrated into the ground plane, and defects in the ground plane disrupt the ground plane's current distribution, altering the transmission line's characteristics. To put it another way, any defect etched in the ground plane beneath the patch adds slot resistance, capacitance, and inductance to the patch's effective capacitance and inductance. This will depend on where the DGS slot is located in the ground. If the ground DGS is closer to the patch than the extended ground DGS, the DGS slot and patch will no longer be able to couple to each other as well. This will change the surface current and, in turn, the field excitation on the antenna's radiating patch.

2.2 Proposed Modelling

This section presents a structured analytical model for a microstrip patch WA operating at 5.8 GHz, designed on a felt substrate with extended DGS. The modeling is to evolve the basic patch antenna configuration into a low cross-polarized, impedance-matched system by incorporating extended DGS. The model addresses key electromagnetic parameters, including LC resonance behavior, surface current disruption, and input impedance tuning, to achieve enhanced polarization purity and return loss performance. Let us model starting with using standard rectangular patch dimensions for length L and width W for the dominant TM_{10} mode.

$$L = \frac{c}{2f_r\sqrt{\epsilon_{eff}}} \tag{1}$$

$$W = \frac{c}{2f_r}\sqrt{\frac{2}{\epsilon_r+1}} \tag{2}$$

Where f_r = 5.8 GHz and ε_r =1.3 (for felt). The ϵ_{eff} is given by:

$$\epsilon_{eff} = \frac{\epsilon_r+1}{2} + \frac{\epsilon_r-1}{2}\left[1 + 12\frac{h}{W}\right]^{-\frac{1}{2}} \tag{3}$$

Where $\epsilon_{eff} \approx 1.3$ and h = height of the substrate (3 mm). These expressions from Eqn. (1)–(3) define the fundamental

geometry of the rectangular patch antenna, which serves as the baseline for further electromagnetic optimization. The subsequent inclusion of an extended DGS in the form of a circular slot significantly alters the surface current distribution and introduces additional reactive components. This modification facilitates improved impedance matching and effectively suppresses cross-polarization components, thereby enhancing polarization purity and achieving better return loss performance. Based on the analytical calculations, the patch dimensions are approximately L≈19 mm and W≈24 mm. The input impedance of the patch antenna, in the absence of DGS, is estimated using Eqn. (4) where the conductance is given by $G_1 = \frac{1}{90}\left(\frac{W}{\lambda_0}\right)$.

$$R_{in} = \frac{1}{2G_1} \tag{4}$$

Here, λ_0 represents the free-space wavelength corresponding to the operating frequency of 5.8 GHz. This formulation provides[22-24] an initial estimate of the antenna's input resistance, which is further refined by the DGS-based tuning for improved radiation performance. The DGS located directly beneath the patch behaves as a band-stop filter and can be represented by a parallel LC resonant circuit. Its impedance is given by Eqn. (5).

$$Z_{DGS}(s) = \frac{1}{sC} + sL \Longrightarrow f_r = \frac{1}{2\pi\sqrt{LC}} \tag{5}$$

Here, the geometrical parameters of the slot length l, width w, and gap g govern the inductance $\mathcal{L}$ and capacitance C of the structure, as Eqn. (6).

$$\mathcal{L} \propto \mu_0.\frac{l}{g} \text{ and } C \propto \varepsilon_0.\frac{w}{g} \tag{6}$$

In general, Eqn. (6) can be described as Eqn. (7).

$$\mathcal{L} = \mu_0.\frac{l}{g} \text{ and } C = \varepsilon_0.\frac{w}{g} \Longrightarrow f_{rDGS} = \sqrt{\frac{g^2}{2\pi\mu_0\varepsilon_0 lw}} \tag{7}$$

In this proposed design, a novel approach is introduced by incorporating DGS elements into an extended ground plane, without direct electromagnetic coupling to the patch. These extended ground DGS elements induce localized perturbations in the surface current paths, minimizing lateral current spread and acting as spatial mode filters. As a result, higher-order and transverse modes are suppressed, leading to reduced cross-polarization. The extended ground DGS can be equivalently modeled as an additional $\mathcal{LC}$ shunt element embedded within the ground plane. This configuration introduces localized loading, which effectively minimizes lateral current spreading and acts as a spatial mode filter. As a result, it suppresses higher-order and transverse resonant modes, thereby contributing to a reduction in cross-polarization. We can approximate this as introducing additional $\mathcal{LC}$ shunt loading to the ground. Here, $\mathcal{L}_{ext}$ is proportional to the slot length, while C_{ext} depends on the width and gap of the extended slot as given in Eqn. (8).

$$Z_{extDGS}(s) = \frac{1}{sC_{ext}} + s\mathcal{L}_{ext} \tag{8}$$

Here, $\mathcal{L}_{ext} \propto$ length of slot in the extended ground and $C_{ext} \propto$ width and gap spacing of slot. The overall input impedance of the antenna is influenced by three parallel components given in Eqn. (9).

$$Z_{total} = Z_{patch} \parallel Z_{DGS} \parallel Z_{extDGS} \tag{9}$$

This composite impedance model facilitates impedance matching, improved return loss, and suppression of unwanted resonant modes. The result is a lower |S11| and enhanced polarization due to suppressed unwanted modes. The cross-polarization is reduced when asymmetric surface current components are suppressed. The cross-polarization arises due to asymmetry in surface current distribution, particularly the transverse component J_y. The cross-polarized electric field component can be analytically approximated by Eqn. 10.

$$E_{\varphi}^{cross} \propto \int J_{x,y} e^{j\beta r} dr \tag{10}$$

where DGS disrupts the J_y component symmetrically in the extended ground results in lower E_{φ}^{cross} compared to the main lobe E_{θ}. To achieve optimal performance, both analytical modeling and full-wave electromagnetic simulations are carried out and cross-validated. The goal is to match the real part of Z_{total} in Eqn. 11.

$$Z_{in}^{match} = R + j(X_{patch} + Z_{DGS} + Z_{extDGS}) \tag{11}$$

Moreover, the proposed circular slot embedded in the extended DGS functions as both a reactive impedance tuning element and a spatial mode filter. This configuration introduces additional inductive and capacitive loading, effectively modifying the surface current distribution to suppress undesired transverse components J_y that contribute to cross-polarization. The circular geometry establishes azimuthally symmetric current paths, mitigating higher-order and surface wave modes through spatial filtering. As a result, the radiated power is more efficiently concentrated in the broadside (boresight) direction, enhancing both gain and impedance matching. The directional gain is given by Eqn. (12)

$$G(\theta,\varphi) = \frac{4\pi U(\theta,\varphi)}{P_{in}} \tag{12}$$

Here $U(\theta,\varphi)$ is the radiation intensity and P_{in} is the total accepted power. Suppressing lateral currents increases U in the broadside direction, leading to higher peak gain. By suppressing lateral surface currents, $U(\theta,\varphi)$ increases in the broadside direction (θ=0°), thereby yielding higher peak gain and reduced cross-polarized radiation. For fine-tuning, practical techniques such as slot loading are applied. Matching elements in circular DGS cavities further help in tuning the impedance and suppressing undesired reactive components. In the proposed design, circular DGS slots and extended ground perturbations, in combination with a patch size of approximately L=19*mm*, W=24*mm*, enable controlled surface current confinement, leading to low cross-polarization and impedance-matched operation around 5.8 GHz.

3. ANTENNA DESIGN

The proposed slot MSPA is designed with a high insulate Felt substrate of thickness 3 mm with a dielectric constant of ε_r=1.36 and a loss tangent of δ=0.02. Felt is a manufactured material produced by the process of matting, condensing, and pressing threads together. Synthetic fibers, such as petroleum-based acrylic or acrylonitrile, or wood pulp-based rayon, as well as natural fibers like wool or animal fur, can be used to produce felt. The material has fire resistance, vibration dampening, sound absorption, and high liquid retention capacity without

susceptibility to wetness. The radiating element consists of a rectangular slot on top of the substrate with a microstrip feed. It also has a circular slot in the center and a circular slot at the ground. This antenna is specifically engineered to resonate at 5.8 GHz, corresponding to a free-space operational wavelength of approximately 51.68 mm. The calculation of the patch width is performed using equations given in the previous section. Thus, the length and width of the patch and antenna have been calculated as above, and the dimensions are given in Table 1. The substrate dimensions are appropriately larger than the patch dimensions, following standard design practices[22] to ensure proper impedance matching, minimal edge effects, and space for feed integration.

Table 1. Physical dimensions of the proposed wearable antenna

Descriptions	Dimensions (mm)
Substrate length	36
Substrate width	40
Patch length	19
Patch width	24
Square slot width	0.3
Square slot length	6
Circular cavity diameter	2
Micro strip feed length	8.5
Micro strip feed width	4
Substrate thickness	3
DGS circular slot radius	1.5

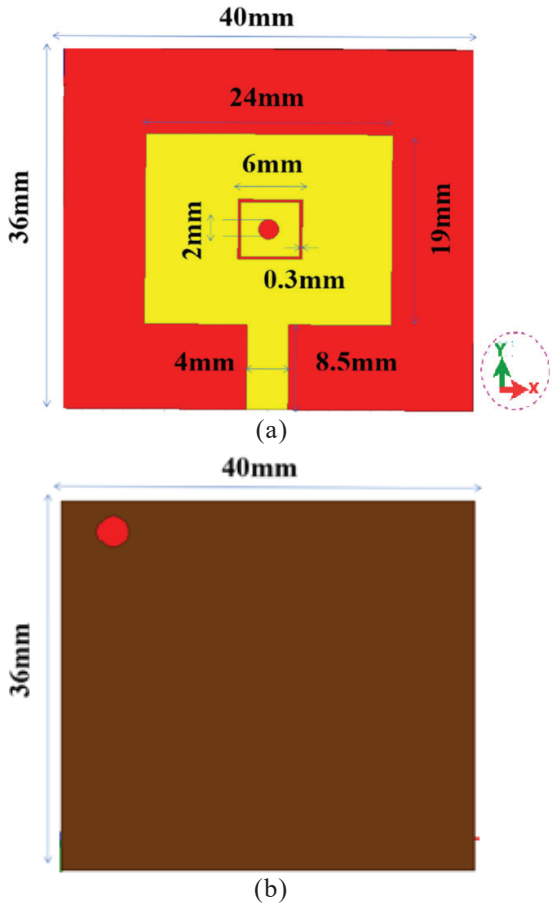

Figure 2. Geometry of the antenna (a) top view; and (b) bottom view.

We design rectangular and square slots within the rectangular patch to stimulate the desired lower resonant frequency, resulting in a reduction in size. A rectangular patch size of 24 mm X 19 mm and a slot of square size with a side of 6 mm with a slot width of 0.3 mm within the patch are designed. We also constructed a circular slot in the extended ground portion. Figure 2 provides a description of the antenna's geometry from both the top view (a) and bottom view (b).

4 ANTENNA PERFORMANCE AND MEASUREMENTS

The simulation is done using HFSS (2020 R2), and the parameters are analyzed and measured. *S*11, or the reflection coefficient, indicates how much power is reflected back from the antenna to the source. It is commonly expressed in decibels (dB) as return loss, where a lower (more negative) value indicates better impedance matching and less reflected power. When *S*11= 0 dB, it means that all the power is reflected back, and none is radiated by the antenna. Conversely, when *S*11= -10 dB, it means that about 10 % of the incident power is reflected back, and approximately 90 % is radiated or absorbed by the antenna. The remaining power was either 'received' or 'delivered' to the antenna. Because low-loss antennas are common, the majority of the power given to the antenna should be radiated. The proposed work achieved the *S*11 of -39 dB with VSWR between 1 to 2 which means our antenna can radiate efficiently. The proposed antenna operates at a 5.8 GHz center frequency, as shown in Fig. 3. Figure 3 describes the simulated and measured *S*11, perfectly matching with the operating frequency. The The antenna's BW (5.51 GHz to 5.93 GHz) is larger than 400 MHz, which meets the ITU-R guideline.

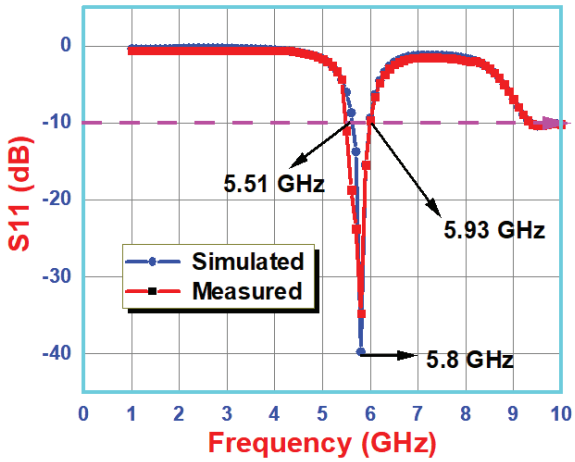

Figure 3. Simulated and measured *S*11 of the proposed antenna.

VSWR is an important parameter for high-frequency antennas, indicating the presence of a mismatch between the antenna and the feed line. In antenna applications, a VSWR value of 2 is generally deemed acceptable, meaning that about 11 % of the power is reflected back, while an ideal antenna would have a VSWR of 1, indicating no reflected power. A low VSWR value signifies that the antenna reflects minimal energy back to the source, ensuring efficient power transfer. Figure 4 describes the measured and simulated VSWR values of various

frequencies ranging from 1 GHz to 10 GHz. At the center frequency of the proposed antenna, the VSWR value is within the range of 1-2 and achieves well-matched transmission at 5.8 GHz. In Fig. 3 and Fig. 4, the *S*11 and VSWR are measured using a VNA and compared. The measured and simulated results are nearly identical, making the antenna more practical.

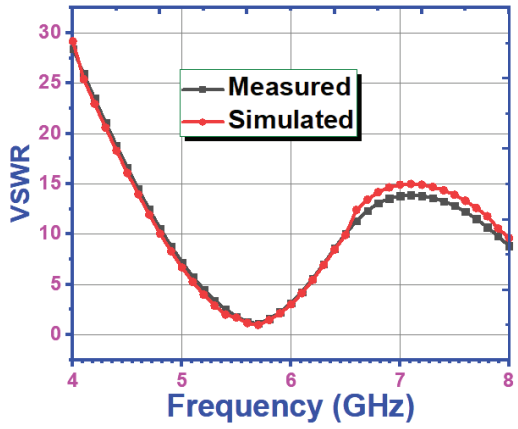

Figure 4. Simulated and measured VSWR of the proposed antenna.

Antenna gain refers to the ratio of the power received by an antenna in the direction of its maximum radiation (on its beam axis) from a distant source, compared to the power that would be received by a hypothetical isotropic antenna, which radiates equally in all directions and has no losses. The larger the region covered by a gain, the higher it is. An antenna with a narrow radio beam is called a high-gain antenna, and it is used to boost signal strength. High-gain directional antennas are employed in scenarios when the direction of the receiving antenna is not constantly fixed. The antenna under consideration attained a gain of 8 dBi at a frequency of 5.8 GHz, rendering it very suitable for use in combat communications applications. With the altering direction angle theta, the gain of the proposed antenna is also tested. The antenna's theta angle is changed from -180 to 180 degrees, and the resulting gain is calculated. The gain for various angles is represented in Fig. 5 and, as expected, the maximum gain is obtained at theta = 0. In Fig. 5, the frequencies ranging from 1 to 10 GHz are shown against the gain. The highest gain of 8 dBi is observed at 5.8 GHz. The

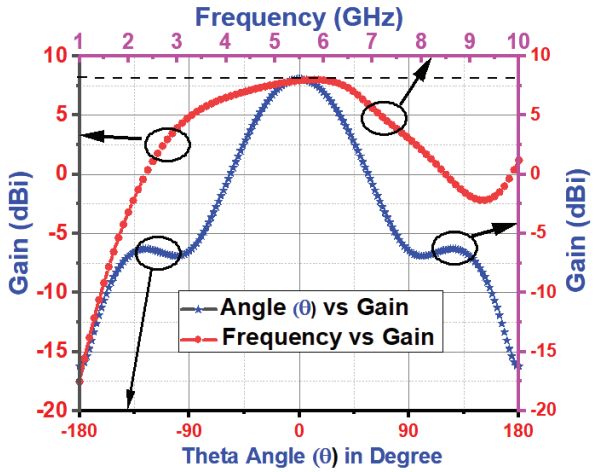

Figure 5. Gain versus frequency and gain variation for different theta angles.

8 dBi gain is achieved by integrating a circular slot DGS and extended ground structure beneath the patch, which suppresses surface wave losses, confines surface currents, and enhances radiation efficiency thereby boosting the overall gain beyond typical patch antenna levels.

This configuration exhibits a significant front-to-back ratio, leading to a strong performance in relation to the application surface, which is an essential characteristic for antennas that operate in close proximity to the human body. The antenna exhibits a front-to-back ratio of 23.89 dB.

The surface current and, as a result, the field excitation on the antenna's radiating patch will change, as will the mutual coupling between the DGS slot and patch. The 3D gain pattern shows that the antenna achieves stronger directivity when the DGS is included in the extended ground, as seen in Fig. 6(b), compared to Fig. 6(a) without the DGS. This improvement is due to the suppression of lateral surface currents, which concentrates more radiated power in the forward (broadside) direction, resulting in higher peak gain and reduced cross-polarization.

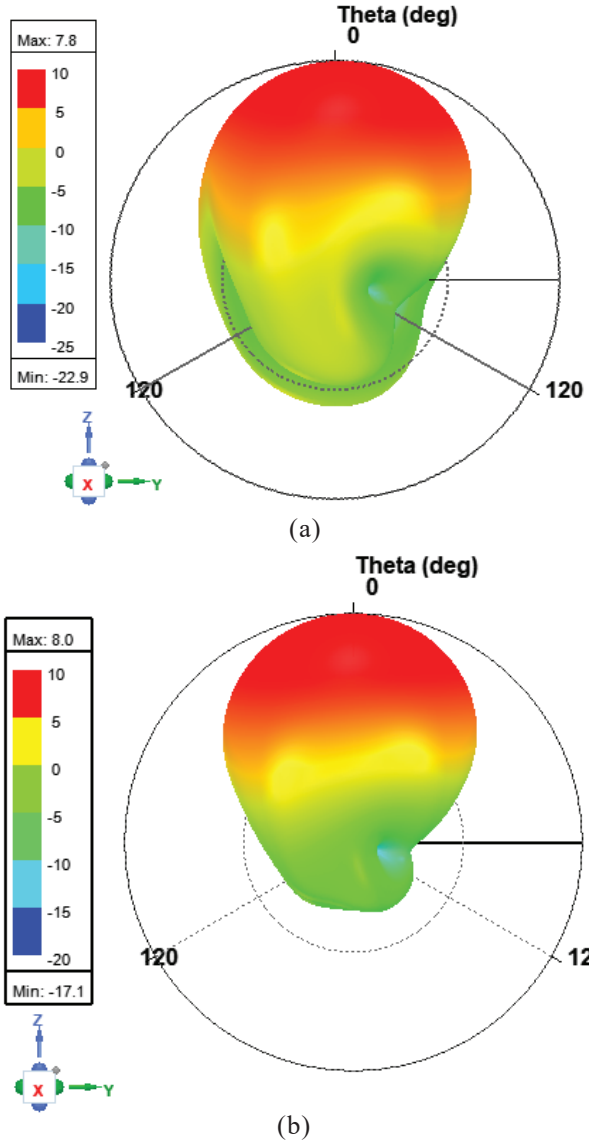

Figure 6. Far-field gain pattern of the proposed antenna (a) without DGS; and (b) with circular slot DGS.

To put it another way, the proposed DGS reduces cross-polarization. To demonstrate this, the proposed antenna's E and H planes will be co-polarized and cross-polarized. Figure 7 shows the E and H-plane co-polarization and cross-polarization of the proposed antenna with and without DGS. The radiation pattern reveals that the proposed DGS reduces cross-polarization. Figure 7 specifies the radiation pattern of the proposed antenna that defines the variation of the power radiated by an antenna as a function of the direction away from the antenna.

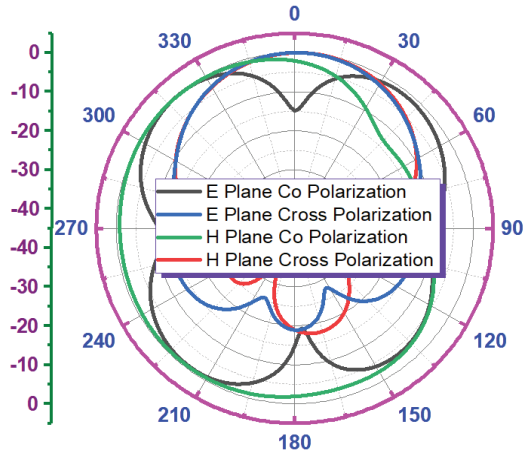

(a)

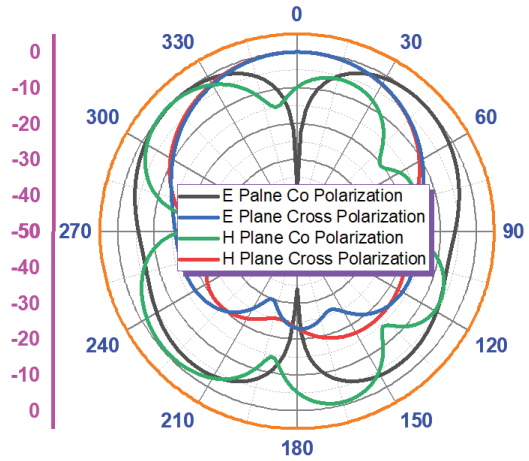

(b)

Figure 7. Co-polarization and cross-polarization patterns in the E and H-planes of the proposed antenna: (a) without DGS; and (b) with DGS.

In Wearable Antenna (WA) applications, a stable and suitably shaped radiation pattern is essential for reliable on-body and off-body communication with spatially distributed sensors. The proposed antenna demonstrates a well-defined directional radiation pattern, enhancing link robustness by maintaining consistent gain and minimizing multipath fading across typical body-worn deployment scenarios. The antenna's radiation efficiency is 84.7 percent, which is greater than average. SAR is a quantification of the upper limit of electromagnetic radiation that a wearable communication antenna in a wireless device can generate. It is calculated using

$$SAR = \frac{\sigma E^2}{\rho}$$

E represents the electric field intensity, σ is conductivity and ρ is the mass density, assuming an input power of 1 Watt. Figure 8 shows the simulated SAR distributions when the antenna is 2 mm, 5 mm, and 7 mm above the human body's skin. Table 2 shows that the greater the distance between the antenna and the human body, the lower the value of SAR.

Table 2. Simulated and measured SAR of the proposed antenna

Distance from arm in mm	2	5	7
SAR (W/Kg) - simulated	1.5	1.49	1.46
SAR (W/Kg) - measured	1.46	1.51	1.48

The SAR values, obtained without the use of any special features, fall within the range of 1.45–1.5 W/kg, below both the IEEE standard threshold of 1.6 W/kg per 1 g tissue and the ICNIRP standard threshold of 2 W/kg per 10 g tissue.

The extended ground's circular slot DGS is a crucial part of the antenna structure. The radius and position of the circular

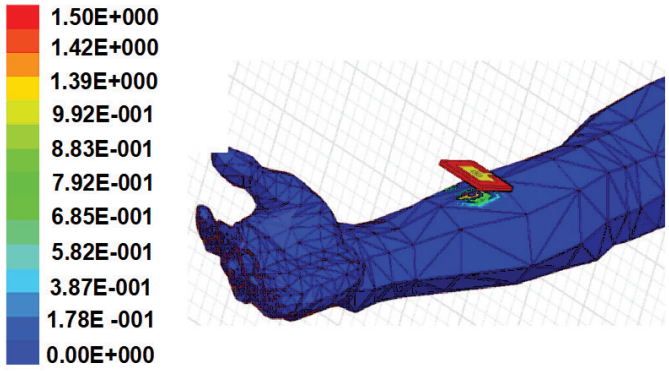

(a)

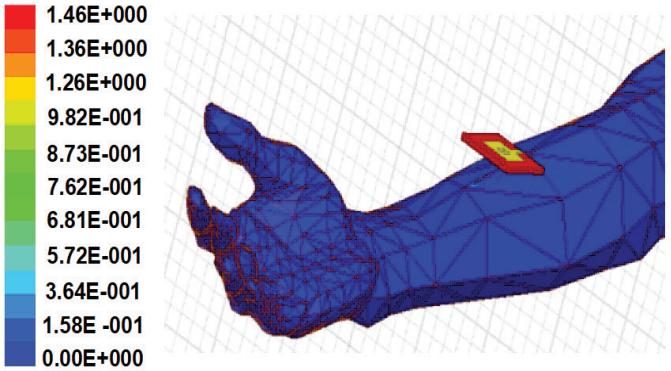

(b)

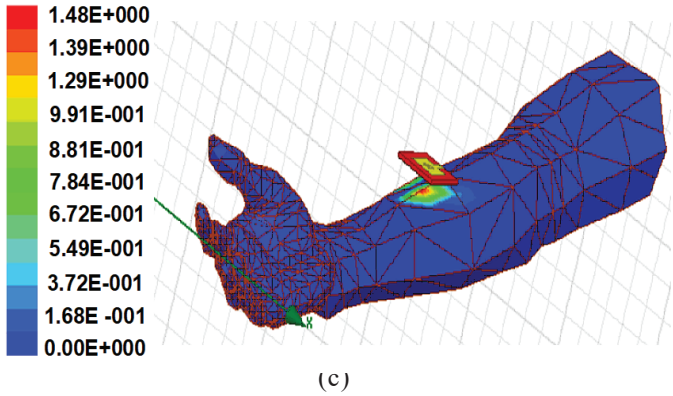

(c)

Figure 8. SAR measurements at various distances (a) 2 mm; (b) 5 mm; and (c) 7 mm.

slot must be investigated. The performance of the circular slot is investigated as the radius of the slot is changed. The radius is changed from 0.75 mm to 2.25 mm, and the *S*11 is determined in decibels. The *S*11 reaches its lowest at a slot radius of 1.5 mm, and the proposed structure employs the same. Figure 9 shows the various radii and their matching *S*11 at 5.8 GHz.

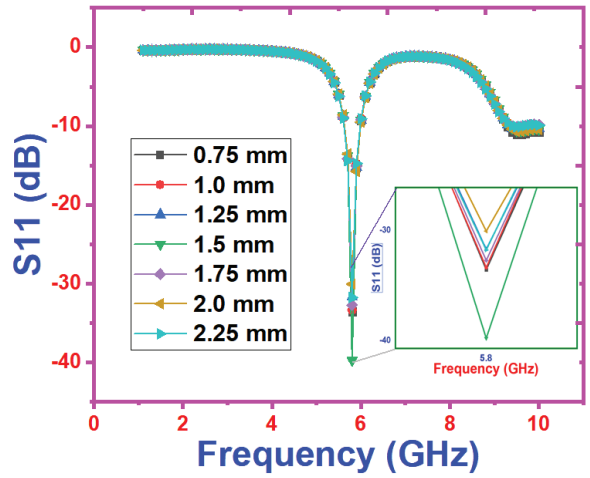

Figure 9. Simulated *S*11 responses for different radii at the operating frequency of 5.8 GHz.

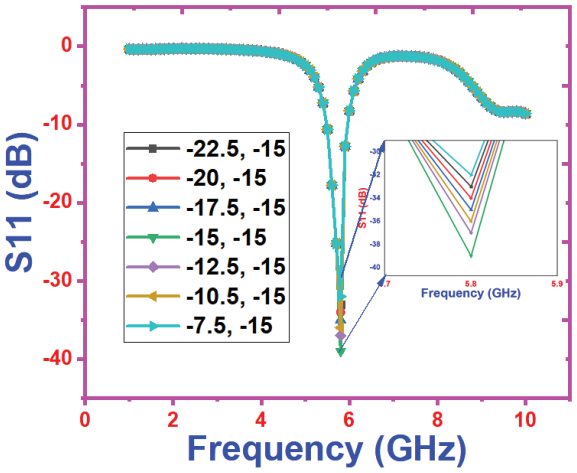

Figure 10. *S*11 matching at 5.8 GHz for varying 'x' locations.

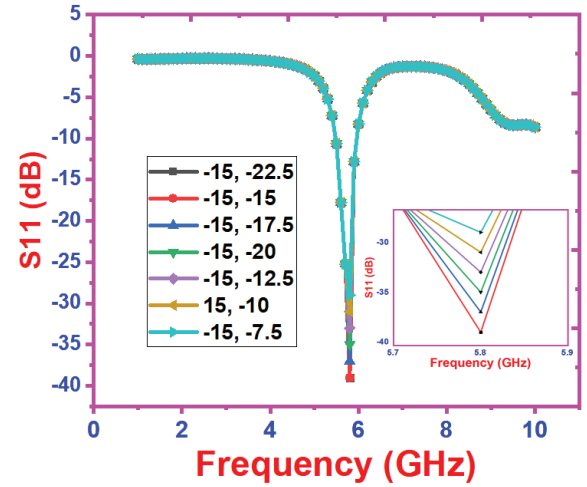

Figure 11. *S*11 matching at 5.8 GHz for varying 'y' locations.

The performance of the circular slot is also tested as the slot's location is adjusted. The antenna's center (0, 0) is moved from -7.5 mm to -22.5 mm in the coordinates "x" and "y" directions, and the *S*11 is measured in decibels. The positions of "x" and "y" changed on their own. Figure 10 depicts only the "x" changes, while Fig. 11 depicts only the "y" changes. In both situations, the *S*11 achieves its lowest point at a slot distance of (-15, -15) mm, and the proposed structure falls into line. The various locations and their matching *S*11 at 5.8 GHz are shown in Fig. 11 and Fig. 12.

The ratio of the total power an antenna radiates to the net power it accepts from the connected transmitter defines radiation efficiency. It is sometimes expressed as a percentage (less than 100) and is frequency dependent. At 5.8 GHz, the proposed antenna has a radiation efficiency of 83.76 percent, as shown in Fig. 12, which plots frequency versus radiation efficiency. The radiated and accepted power of the proposed antenna is well matched to the frequency of operation. In all cases, the incident power is taken as one watt. From these, the proposed antenna works well within the required frequency range.

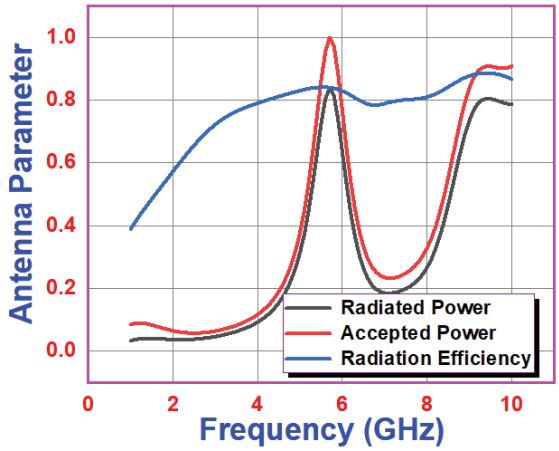

Figure 12. Radiated power, accepted power, and radiation efficiency of the proposed antenna at 5.8 GHz.

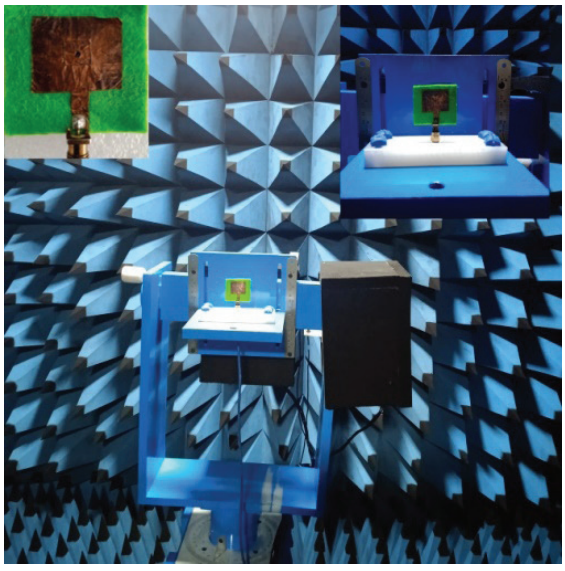

Figure 13. Photograph of the fabricated prototype of the proposed antenna and its measurement setup inside the anechoic chamber.

4.1 Model of the Proposed Antenna Prototype

The antenna was manufactured based on the aforementioned design structure. The photograph of the prototype antenna and the measurement set-up in the anechoic chamber is presented in Fig. 13. In the anechoic chamber, the *S*11 and VSWR are measured using the prototype model. The observed parameters were compared to the simulated results, which were determined to be identical. The prototype's *S*11 is -35.65 dB, and the obtained VSWR is 1.26 as plotted in Fig. 3(a) and Fig. 4.

The overall performances are tabulated and compared to similar works from the previous few works and given in Table 3. The performance of the proposed antenna is better in several aspects, according to the comparison. The performances in terms of *S*11, SAR, gain, size, and BW are compared. The VSWR drops from roughly 1.065 to 1.01 when return loss increases from -30 dB to -40 dB. A better impedance match is indicated by this decrease in VSWR, which maximizes power supply to the load or antenna and reduces power reflection. Higher VSWR corresponds directly to higher system performance and efficiency. The matching gets better, and the impedance mismatch gets smaller as return loss goes down. Reflexion coefficients of 0.01 and 0.032 indicate a notable improvement in matching. The system reflects 0.1 % of the power with a return loss of -30 dB, but only 0.01 % at a loss of -40 dB, suggesting that more power was successfully transmitted to the load. The following relations Return loss in dB = $-20\log_{10}(|\Gamma|)$ and VSWR $= \frac{1-|\Gamma|}{1+|\Gamma|}$ are used for the above descriptions. In these relation, Γ corresponds to reflexion coefficients.

To evaluate the antenna's performance under realistic operational conditions, S11 and Voltage Standing Wave Ratio (VSWR) measurements were conducted with the antenna mounted directly on a human subject. These measurements, depicted in Fig. 14, quantify the impact of the loss, on the antenna's input impedance and matching characteristics. The inclusion of a photographic inset in Fig. 14 documents the physical test configuration and ensures reproducibility of the experimental setup. Despite the detuning typically introduced by proximity to biological tissue, the antenna exhibited stable operation, maintaining *S*11 below –10 dB and VSWR < 2 across the designated frequency band. These results validate the antenna's impedance robustness and its viability for body-centric wireless communications. The on-body performance demonstrates minimal degradation relative to free-space

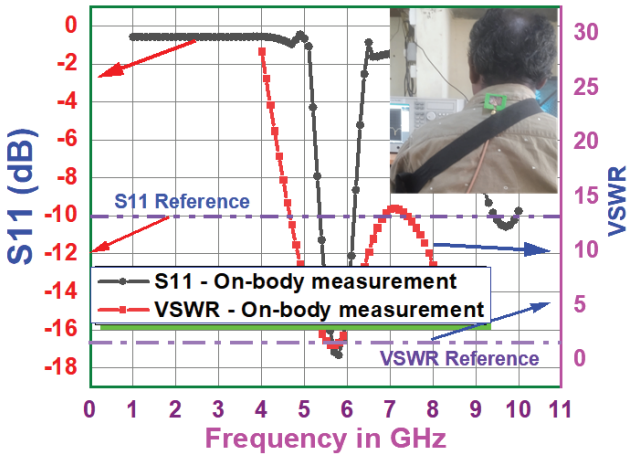

Figure 14. Measured *S*11 and VSWR of the Proposed WA on the human body. Inset: experimental setup (photograph) showing on-body placement.

Table 3. Performance Comparison Previous Works

Reference of previous work	*S*11 dB	SAR	Gain dBi	Size	Frequency GHz	BW
[8], 2020	-30	4.51W	3.5	R=35 mm	2.45	25 MHz
[9], 2020	-22	0.118 W/kg (1 g tissue) & 0.0536 W/kg (10 g tissue)	3.5	0.15λ×0.1λ×0.004λ (@ 2.45 GHz)	5.85	220
[10], 2020	-37	1.02 W/kg (1 g tissue) and 0.947 W/kg (10 g tissue)	5.0 -6.1	0.05 λ (@5.8 GHz)	5.8	NA
[11], 2020	-35	0.13-10 g	3.31	42mm × 25mm	5.5	NA
[12], 2020	-30	SAR 0.722 W/kg (1 g tissue) 1.6 W/kg (IEEE C95.1-2005 standard).	7.7	70 mm×70 mm	WiMAX (3.4–3.6)	200 MHz
[13], 2021	-42	NA	2.76	1.76 cm×1.76 cm	5.8	NA
[14], 2021	-32	0.0257 w /kg	7.47	45×45×2.4 mm^3	2.45	NA
[15], 2021	-12.5	2 W/kg averaged over 10 g	NA	15.8×7 cm	875	NA
[16], 2021	-13	NA	4.76	38×19	5.3	NA
[4], 2024	-20	1.6 W/kg (U.S. standard) & 2W/kg (EU-standard)	8.9	28×28 mm	8.2	7.73–11.3 GHz
[3], 2024	-35	--	--	60×60	18	13.1 - 31.13 GHz
[2] , 2024	-25	1.58 W/kg, averaged over 10 g of tissue with an input power of 0.5 W	6.2	31×20	4.5	-
[5], 2024	-30	The peak SAR value - 1.48 W/kg (over 1 g of tissue) and 0.27 W/kg (10 g of tissue)	7.14	10.5×21.5	17	3.1–34.5 GHz
This work	**-39.5**	**Distance from arm in 2 mm SAR (W/Kg) = 1.5**	**8**	**36 × 40 mm**	**5.8**	**400 MHz**

measurements, indicating effective electromagnetic integration for wearable deployment.

5. CONCLUSION

This work presents a flexible DGS slot antenna designed for tactical operational communications in the battlefield. The proposed flexible antenna incorporates an extended ground DGS with a circular aperture. To achieve an 8 dBi gain, the circular slot DGS antenna was consciously placed to minimize return loss. This antenna operates at the center frequency of 5.8 GHz in the band of 5.51 GHz to 5.93 GHz with a desirable radiation pattern suitable for battlefield communications applications, with an impedance BW of 400 MHz. The results of the simulation and the measurements are compared. When the overall properties of the suggested antenna were compared to those of other recent studies, it was learned that it is best suited for ISM band applications that require 5.725 GHz to 5.875 GHz with a center frequency of 5.8 GHz and 150 MHz BW. Its SAR value is lower than the IEEE standard for antenna parameters that are acceptable.

REFERENCES

1. Giftsy ALS, Kommuri UK, Dwivedi RP. Flexible and wearable antenna for biomedical application: progress and opportunity. IEEE Access. 2024;12:90016–40. doi:10.1109/ACCESS.2023.3343154.
2. Samal PB, Chen SJ, Fumeaux C. 3D-corrugated ground structure: A microstrip antenna miniaturization technique. IEEE Trans Antennas Propag. 2024;72(5):4010–22. doi:10.1109/tap.2024.3385909.
3. Celenk E, Lynch C, Tentzeris MM. An ultra-wideband all-textile metamaterial absorber for Ku, K and Ka band applications. IEEE Antennas Wirel Propag Lett. 2024:23(6):1–5. doi:10.1109/lawp.2024.3369971.
4. Baudh RK, Sahu S, Parihar MS, Kumar VD. A wideband circularly polarized all textile on-body antenna for defense applications. IEEE Trans Circuits Syst II Exp Briefs. 2024;71(2):567–71. doi:10.1109/tcsii.2023.3308213.
5. Bhatt PN, Pandhare R. A tensile wearable SHF antenna with efficient communication in defense beacon technology. Def Technol., 2024;41(9):198–210. doi:10.1016/j.dt.2024.05.005.
6. Lago H, Soh PJ, Jamlos MF, Shohaimi N, Yan S, Vandenbosch GAE. Textile antenna integrated with compact AMC and parasitic elements for WLAN/WBAN applications. Appl Phys A., 2016;122(12):6. doi:10.1007/s00339-016-0575-9.
7. Zhu S, Langley R. Dual-band wearable textile antenna on an EBG substrate. IEEE Trans Antennas Propag. 2009;57(4):926–935. doi:10.1109/TAP.2009.2014527.
8. Sun H, Hu Y, Ren R, Zhao L, Li F. Design of pattern-reconfigurable wearable antennas for body-centric communications. IEEE Antennas Wirel Propag Lett., 2020;19(8):1385–1389. doi:10.1109/LAWP.2020.3002016.
9. Le TT, Yun TY. Miniaturization of a dual-band wearable antenna for WBAN applications. IEEE Antennas Wirel Propag Lett., 2020;19(8):1452–1456. doi:10.1109/LAWP.2020.3005658.
10. Zu HR, Wu B, Zhang YH, Zhao YT, Song RG, He DP. Circularly polarized wearable antenna with low profile and low specific absorption rate using highly conductive graphene film. IEEE Antennas Wirel Propag Lett., 2020;19(12):2354–2358. doi:10.1109/LAWP.2020.3033013.
11. Pei R, Leach M, Lim EG, Wang Z, Wang J, Wang Y, et al. Wearable belt antenna for body communication networks. IEEE Antennas Wirel Propag Lett., 2020;19(12):2043–2047. doi:10.1109/LAWP.2020.3021677.
12. Yang H, Liu X. Wearable dual-band and dual-polarized textile antenna for on- and off-body communications. IEEE Antennas Wirel Propag Lett., 2020;19(12):2324–2328. doi:10.1109/LAWP.2020.3032540.
13. Hasni U, Piper ME, Lundquist J, Topsakal E. Screen-printed fabric antennas for wearable applications. IEEE Open J Antennas Propag., 2021;2:591–598. doi:10.1109/OJAP.2021.3070919.
14. Ashyap AYI, Dahlan SHB, Abidin ZZ, Rahim SKA, Majid HA, Alqadami ASM, et al. Fully fabric high impedance surface-enabled antenna for wearable medical applications. IEEE Access., 2021;9:6948–6960. doi:10.1109/ACCESS.2021.3049491.
15. Singh RK, Michel A, Nepa P, Salvatore A, Terraroli M, Perego P. Compact and wearable Yagi-like textile antennas for near-field UHF-RFID readers. IEEE Trans Antennas Propag., 2021;69(3):1324–1333. doi:10.1109/TAP.2020.3030944.
16. Elias BBQ, Soh PJ, Al-Hadi AA, Akkaraekthalin P. Gain optimization of low-profile textile antennas using CMA and active mode subtraction method. IEEE Access., 2021;9:23691–23704. doi:10.1109/ACCESS.2021.3056905.
17. Sandhya M, Anjaneyulu L. Robust, efficient and low profile fractal enabled EBG incorporated wearable antenna for WLAN standards. Def Sci J., 2022;72(3):429–440. doi:10.14429/dsj.72.17674.
18. Ahirwar S, Rao AP, Chakravarthy M. Design of a low profile Archimedean spiral antenna using compact defected ground structure as a reflector. Def Sci J. 2023;73(5):572–581. doi:10.14429/dsj.73.17751.
19. Bhavani S, Shanmuganantham T. Wideband fabric antenna for ultra wideband applications for medical applications. Def Sci J., 2022;72(6):864–872. doi:10.14429/dsj.72.17919.
20. Modak S, Farooq U, Lokam A. Circularly polarized MIMO antenna system for millimeter wave 5G applications using characteristic mode theory. Int J Commun Syst., 2025;38(5):e70017. doi:10.1002/dac.70017.
21. Modak S, Kaim V, Khan T, Kanaujia BK, Matekovits L, Rambabu K. Design and performance measurement of worn-on-body instrumental ultra-miniaturized UWB wearable patch for e-health monitoring. IEEE Access.,

2024;12:25719–25730.
doi:10.1109/ACCESS.2024.3365938.
22. Khandelwal MK, Kanaujia BK, Kumar S. Defected ground structure: fundamentals, analysis, and applications in modern wireless trends. Int J Antennas Propag. 2017;2017:1–22.
doi:10.1155/2017/2018527.
23. Caloz C, Okabe H, Iwai T, Itoh T. A simple and accurate model for microstrip structures with slotted ground plane. IEEE Microw Wirel Compon Lett., 2004;14(3):127–129.
doi:10.1109/LMWC.2003.822564.
24. Gupta SK, Sharma A, Kanaujia BK, Rudra S, Mishra RR, Pandey G. Orthogonal slit cut stacked circular patch microstrip antenna for multiband operations. M*icrowave Opt Technol Lett*. 2013;55(4):873–882.
doi:10.1002/mop.27416.

CONTRIBUTORS

Dr S. Anand obtained his PhD degree from Anna University Chennai and working as Professor, Electronics and Communication Engineering, Mepco Schlenk Engineering College, Sivakasi, Tamil Nadu, India. His current research interests include: Antenna design and image processing.
In the current study he spearheaded the research design, ensuring the alignment of the study's objectives with the experimental approach, and executed the key experiments.

Dr Sivasankar Ganesan obtained M.E. in Embedded and Real-time Systems from Anna University working as a Assistant Professor (Sr. Grade), Department of Mechanical Engineering, Amrita School of Engineering, Coimbatore, Amrita Vishwa Vidyapeetham, India. His areas of interest are robotics and embedded systems.
In the current study he contributed essential methodological expertise, guiding the data analysis process and ensuring the accuracy of the results.

Ms D. Sujitha is an UG student at Department of ECE, Mepco Schlenk Engineering College, Sivakasi.
In the current study she played a pivotal role in developing the theoretical framework, providing context through a comprehensive literature review that grounded the study

Ms S. Vigneshwari is an UG Student at Department of ECE, Mepco Schlenk Engineering College, Sivakasi, India.
In the current study she oversaw the manuscript preparation, ensuring coherence in writing, and was instrumental in securing the necessary funding to support the research.